

# Measurement of Optical Cavity Properties in Semiconductor Lasers by Fourier Analysis of the Emission Spectrum

Daniel Hofstetter and Robert L. Thornton, *Member, IEEE*

**Abstract**—We present several observations on a novel method for the evaluation of the internal loss properties in semiconductor lasers. The method we use involves Fourier analysis of the Fabry–Perot mode spectrum when operating the device below lasing threshold. The observation of various structural features in the Fourier transform domain allows us to extract important information on the laser cavity. As one example, the amount of cavity propagation loss/gain, or net gain, can be derived from the decay rate of harmonics of the Fourier spectrum. A comparison between experimental and calculated gain versus wavelength data for lasers fabricated in the AlGaAs, AlGaInP, and AlGaInN material systems will be given. As a second example, this method also allows the identification of the density and strength of intracavity scattering centers. This is an important capability for the fabrication of blue diode lasers in the gallium-nitride material system.

**Index Terms**—Emission spectrum, Fourier analysis, gain spectrum, laser cavity, semiconductor lasers.

## I. INTRODUCTION

THE characterization of laser cavities in terms of internal loss or gain is a research topic of ongoing relevance and importance, especially with regard to the development of new laser materials and designs in the short-wavelength range of the spectrum. An elegant method to determine the net gain is based on a measurement of the Fabry–Perot (FP) fringe contrast  $m$  in the spectrum [1]–[3]. The contrast is defined as  $m = (I_{\max} - I_{\min}) / (I_{\max} + I_{\min})$ . This method, commonly referred to as the Hakki–Paoli method, is very effective for low  $Q$  cavities when  $m$  is significantly less than one. However, this method starts to be inaccurate for higher  $Q$ -factor cavities with  $m$  approaching 1, in which case the spectrum evolves into a series of Dirac-delta functions.

In this paper, we show a new method to measure the optical gain of semiconductor laser cavities. The detailed analysis of Fourier transformed subthreshold spectra [4], [5] allows us to determine the cavity propagation loss/gain which is synonymous with the net gain. The Fourier transformation

of the FP fringe pattern results in a spectrum containing the fundamental FP frequency, related to the cavity length, plus harmonics thereof [6]. As will be shown below, the wavelength-averaged cavity propagation loss/gain is related to the ratio between the Fourier coefficients of adjacent harmonics [7], [8]. Therefore, by knowing the internal cavity losses and using the propagation loss/gain, or the mirror reflectance as fitting parameters to match theoretically transformed spectra to experimental data, we can, for instance, obtain a measurement of the gain spectrum or of the transparency current level. For a certain class of devices like high- $Q$ -cavity lasers, the Fourier transform method is superior to the FP contrast measurement method [1], [2] in the respect that it continues to be useful as  $m$  approaches unity and in fact is limited only by the resolution of the spectrometer used. In addition, if the spectrometer resolution is sufficiently high, it potentially allows the correct determination of the FP fringe contrast even if both TE/TM mode families are present in the spectrum. In such a case, the beating between the two mode sets would allow the use of the Hakki–Paoli method only by performing two separate measurements of the TE/TM mode spectra. Furthermore, by investigating the part of the transformed spectrum which corresponds to optical path lengths shorter than the cavity length, it is possible to obtain important information about the quality of the optical waveguide. This is critical in the nitrides because their large lattice mismatch to available substrates causes the material to crack or to form hexagonal pits and nanopipes, leading to severe scattering loss within the laser cavity [9]. The use of Fourier transforms of the spectrum reveals information about the spatial distribution of scattering centers along the laser cavity in a much more timely way than transmission electron microscopy [10], [11]. An additional feature of our technique is that it works equally well on optically pumped samples [12]–[15] and on electrically pumped ones [16], [17].

In this paper, we will first provide physical models for the technique which we have used. We will then develop the theoretical tools which are necessary for the understanding of Fourier transforms of semiconductor laser emission spectra. We will thereby gain a deep understanding about the nature of the various features in a transformed spectrum and prepare ourselves for interpretations and limits of this method. In the third part, we show the experimental setup which was used to carry out the experiments. The fourth section of this paper describes experimental results we obtained from infrared, red,

D. Hofstetter was with the Xerox Palo Alto Research Center, Palo Alto, CA 94304 USA. He is now with the Physics Department, Neuchâtel University, CH-2000 Neuchâtel, Switzerland.

R. L. Thornton was with the Xerox Palo Alto Research Center, Palo Alto, CA 94304 USA. He is now with Maxtek Corporation, Beaverton, OR 97075-0428 USA.

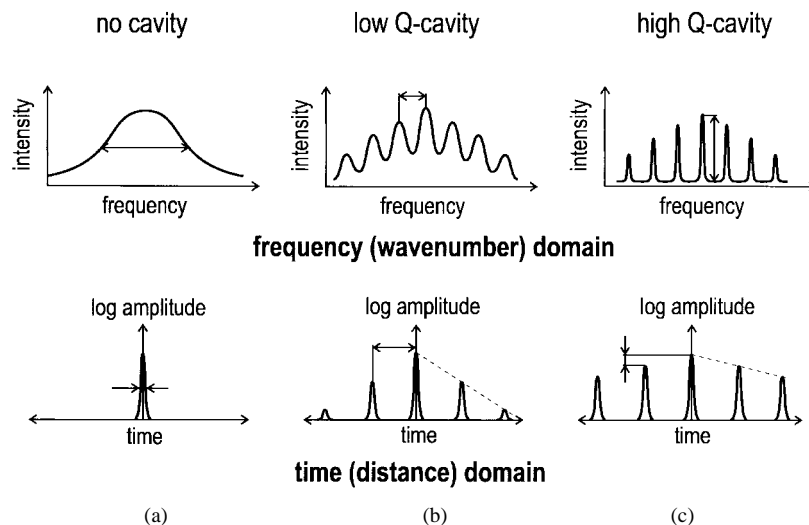


Fig. 1. Intensity versus frequency spectra and their Fourier transforms for light emitters with three representative cavity configurations.

and blue light emitters of different kinds. In the conclusions, we will give an outlook on future experiments and how they might influence ongoing semiconductor laser research.

## II. PHYSICAL MODEL

The physical model for our method is based on the Fourier transform relationship between the frequency response of a system and the time-domain impulse response, or Green's function, of that system. When a laser cavity is excited below threshold, the spectrally broad emission observed is equivalent, in the time domain, to stimulating the cavity with a delta-function impulse. This is equivalent to stating that the Fourier transform of a broad Gaussian-like frequency response is a narrow Gaussian-like temporal response. In Fig. 1(a), we show the Fourier transform pair corresponding to an LED-like emission with no cavity resonance.

If this same LED-like broad emitter is placed into a low- $Q$ -resonant cavity as in Fig. 1(b), we will observe a weak modulation superimposed on the broad LED emission in the frequency domain, which will correspond, in the transform (time) domain to a series of delta functions with rapidly decreasing amplitudes. The separation between these peaks in the time domain corresponds to the round-trip time of the resonant cavity, and the decay of these peaks is related to the averaged round-trip loss in the cavity.

As we decrease the loss in the cavity, or increase the  $Q$ -factor of the cavity as in Fig. 1(c), we see stronger interference with sharper peaks in the frequency domain. Equivalently, in the transform domain, we see a more slowly decaying series of delta functions corresponding to the lower round-trip loss in the laser cavity. As a result, we would expect that by performing a Fourier transform analysis on subthreshold laser emission at varying currents, we can extract information regarding the losses in the laser cavity.

It should be mentioned that throughout this paper, we will show spectra which, in the time domain, extend to both negative and positive infinity. This is an apparent violation of causality, in that the response to an impulse cannot appear

in time before the appearance of the impulse itself. It is the result of nonrigorous treatment of the complex nature of the true impulse response function. Causality would dictate that the frequency-domain information, which we measure in a spectrum as purely real, must, in fact, consist of a real and imaginary part which are a Hilbert transform pair [18]. For the purpose of the analysis that we undertake here, however, no new information is provided by the Hilbert transformation. The reason why we see in the time-domain harmonic peaks for both positive and negative times is that we have omitted the phase information in the original intensity versus frequency spectrum. However, since we know that the transform of a real function, which fulfills causality in the time domain, consists of a real and imaginary function which are Hilbert transforms of each other, it seems to be quite possible to construct the missing phase information from the measured intensity versus frequency spectrum. Therefore, in this paper, we will forego Hilbert transformation at the expense of symmetric noncausal impulse responses.

The true power of the transform analysis, and the time-domain picture, is appreciated when we consider a cavity containing a perturbation, such as a crack or some other scattering center. In this case, the frequency-domain emission spectrum will exhibit amplitude modulations which, if sufficiently simple, will appear as beat frequencies superimposed on the spectrum. In the transform domain, these will be evident as temporal features at times other than integral multiples of the cavity round-trip time. The position of these peaks relative to the cavity round-trip peaks will contain information on the position of the perturbation within the cavity. This is shown schematically in Fig. 2.

Thus, it is seen that the ability to excite a resonant cavity with a broad band LED-like spectrum is in many ways equivalent to being able to excite that cavity with an extremely short (and in practice nontrivial to generate) probe pulse. Performing a Fourier transform on the modulated spectrum is therefore equivalent to watching the evolution of response pulses to this effective probe pulse. This reveals the internal structure of the resonant cavity.

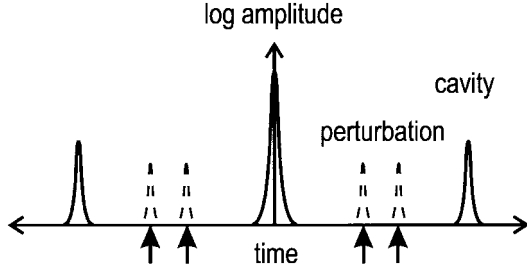


Fig. 2. Effect of an intracavity reflection on the Fourier transformed spectrum. The additional peak pairs due to the intracavity reflection are marked by arrows.

### III. THEORY

We will now develop a rigorous analysis of the relationship between the frequency-domain and time-domain responses. In so doing, it is important to choose the appropriate pair of Fourier transform variables. Although we usually measure, in an experiment, the intensity as a function of wavelength, it is much more convenient to perform the mathematical analysis based on intensity versus wavenumber data,  $I(\beta)$ , where  $\beta = 2\pi/\lambda$ . This will ultimately provide us with a more direct relationship between spectral frequency and time. When doing Fourier transforms on these data, we obtain intensity versus optical path length,  $\bar{I}(d)$  information. The conjugate variables are, therefore, wavenumber  $\beta$  and optical path length  $d$ . These variables can be related to another pair of physically meaningful transform variables, optical frequency  $\omega = \beta c$ , and transit time  $t = d/c$ , with  $c$  being the speed of light. We choose to develop this mathematical formalism based on the former pair.

For generality, we will derive an analytical expression for the Fourier transform of an active or passive FP resonator spectrum. If the considered FP resonator has a length  $L$  and consists of a piece of material with parallel facets, refractive index  $n$ , and absorption index  $k$ , which both do not depend on the wavelength or wavenumber, then the transmitted electrical field amplitude experiences multiple reflections between the facet mirrors. It can be calculated as a geometrical series as given by

$$A(\beta) = (1 - R \cdot e^{2i\psi}) \cdot \sum_{m=0}^{\infty} (R \cdot e^{2i\psi})^m \cdot e^{-2kL(m+1/2)\beta} \cdot e^{2inLm\beta} \quad (1)$$

where  $\beta = 2\pi/\lambda$  is the wavenumber,  $R = [(n-1)^2 + k^2]/[(n+1)^2 + k^2]$  is the power reflectance of the facets, and  $\psi = \arctan(-2k/n^2 + k^2 - 1)$  is the phase change of the light due to the facet reflection. Obviously, the expansion into a converging geometrical series fails if  $R \cdot e^{-2kL\beta} \geq 1$ ; for active resonators, this means that the expansion works only below lasing threshold. For the following calculations, we assume that there is no dispersion in the refractive and

the absorption index within the wavelength range of interest. Furthermore, we consider only incidence angles of  $90^\circ$ , a relatively narrow wavenumber range ( $\Delta\beta = \beta_{\max} - \beta_{\min} \ll \beta$ ), and small absorption index values ( $k \ll n$ ). As a result of these assumptions, we can replace in (1) the variable term  $\exp(-2kLm\beta)$  by the constant term  $\exp(-2kLm\beta_0)$ . From (1), we can thus calculate the transmitted intensity according to (2), shown at the bottom of the page.

Especially for high values of the finesse  $F$ , defined by  $F = \pi\sqrt{R}/(1-R)$ , this function can be recognized as an Airy function. With the above assumption  $k \ll n$ , it follows that  $\arctan(-2k/(n^2+k^2-1)) \approx 0$ , and then (2) simplifies to

$$I(\beta) = \frac{(1-R)^2 \cdot e^{-2kL\beta_0}}{(1-R \cdot e^{-2kL\beta_0})^2 + 4R \cdot e^{-2kL\beta_0} \cdot \sin^2(nL\beta)} \quad (3)$$

As shown in the book of Hecht and Zajac [19], a single transmission maximum of the Airy function has a shape which is approximately a Lorentzian lineshape. It can be shown more generally that the Airy function is in fact identically equal to the summation of an infinite series of Lorentzian functions with a constant separation [20]. As this is a critical identity for the analysis that follows, we present a rigorous mathematical derivation here.

Starting from (2), we can do some rearrangements; (3) then becomes

$$I(\beta') = \frac{C_1}{1 + C_2 \cdot \cos(2\pi\beta')} \quad (4)$$

where  $\beta' = (nL\beta)/\pi$ , and, in addition,

$$C_1 = (1-R)^2 \cdot \frac{e^{-2kL\beta_0}}{1 + R^2 \cdot e^{-4kL\beta_0}}$$

and

$$C_2 = -2R \cdot \frac{e^{-2kL\beta_0}}{1 + R^2 \cdot e^{-4kL\beta_0}} \quad (5)$$

These constants can be written somewhat simplified as

$$C_1 = \left(\frac{1-R}{\sqrt{2R}}\right)^2 \cdot \frac{1}{\cosh(2kL\beta_0 - \ln(R))}$$

and

$$C_2 = \frac{-1}{\cosh(2kL\beta_0 - \ln(R))} \quad (6)$$

By using complex functional theory arguments, which will be outlined below, one can show that the function shown in (3) is identical to a new one consisting of an infinite series of Lorentz peaks, as represented by

$$J(\beta') = \frac{C_1}{a\pi \cdot \tanh(2a\pi)} \cdot \sum_{m=-\infty}^{\infty} \frac{1}{1 + \left(\frac{\beta' - m}{a}\right)^2} \quad (7)$$

where the parameter  $a$  is determined through the relation  $a = (2\pi)^{-1} \operatorname{arcosh}|1/C_2|$ , which is identical to  $a = (2\pi)^{-1}$ .

$$I(\beta) = |A(\beta)|^2 = A(\beta) \cdot A^*(\beta) = \frac{(1-R)^2 \cdot e^{-2kL\beta_0} + 4 \sin^2(\psi)}{(1-R \cdot e^{-2kL\beta_0})^2 + 4R \cdot e^{-2kL\beta_0} \cdot \sin^2(\psi + nL\beta)} \quad (2)$$

$(2kL\beta_0 - \ln(R))$ . The mathematical way to prove that (4) and (7) are the same is to consider their respective complex functional natures as follows.

A complex function is said to be analytic or holomorphic if its derivative exists at each point of the region  $G$ ; in addition, it is said to be entire if the derivative exists in the entire complex plane. Meromorphic functions are holomorphic except for the presence of poles. Under the above definitions,  $I(\beta')$  in (4) and  $J(\beta')$  in (7) are meromorphic functions in the complex plane. When defining parameter  $a$  in the above way, the functions  $I(\beta')$  and  $J(\beta')$  have the same poles, and at these poles, they have identical singularity parts. As a result of this, the difference function  $F(\beta') = I(\beta') - J(\beta')$  no longer has any poles;  $F(\beta')$  is therefore an entire function. In addition, both  $I(\beta')$  and  $J(\beta')$  have the same periodicity  $nL/\pi$ , and both approach zero regularly when the imaginary part goes toward infinity, meaning that they both are bound. Therefore, their difference  $F(\beta')$  is a bound function as well. The theorem of Liouville states that the only entire function  $F(\beta')$  which is bound in the entire complex plane is the constant function  $F(\beta') = \text{constant}$ . Since the function  $F(\beta')$  vanishes when its imaginary part approaches infinity, this constant must be zero. Therefore,  $I(\beta')$  and  $J(\beta')$  must be, in fact, identical.

The most important consequence of this is that the series of Lorentz functions  $J(\beta')$  is much easier to Fourier-transform than the Airy function  $I(\beta')$ . Since we have outlined the mathematics to perform the Fourier transform of  $I(\beta')$  in [17], we will omit this part here and give only the final result

$$\overline{I(d)} = |1 - R \cdot e^{2i\psi}|^2 \cdot \sum_{m=0}^{\infty} \sum_{\ell=0}^{\infty} \frac{R^{\ell+m} \cdot e^{-2i\psi(\ell-m)}}{[kL(\ell+m+1) + i(\pi d + nL(\ell-m))]} \quad (8)$$

In contrast to the tedious derivation of (8), the Fourier transform of  $J(\beta')$  is very straightforward if one realizes that  $J(\beta')$  is a convolution of an infinite series of  $\delta$  functions and a Lorentz function. The desired transform is then given by the product of the series of  $\delta$  functions and the transform of the Lorentz peak, which is a symmetric exponential decay function

$$\overline{I(d')} = 2\pi a \cdot e^{-2\pi a|d'|} \cdot \sum_{m=-\infty}^{\infty} \delta(d' - m). \quad (9)$$

Here, the conjugate variable  $d'$  is defined via  $d' = d\pi/nL$ . This function consists of an infinite series of  $\delta$  functions, which are arranged symmetrically to the origin. Since we are interested only in the amplitude of this complex function, we can omit the phase factor, which is due to the translation along the  $x$  axis. We get therefore a constant ratio between the amplitudes of adjacent harmonics, and this ratio is given by the following relation:

$$\begin{aligned} r &= \exp(-2\pi a) \\ &= \exp\left(ar \cosh\left(\frac{1 + R^2 \cdot e^{-4kL\beta_0}}{2R \cdot e^{-2kL\beta_0}}\right)\right) = R \cdot e^{-2kL\beta_0}. \end{aligned} \quad (10)$$

Although the complex functions in (9) and (10) consist—in general—of amplitude and phase, we will plot the amplitude

only for the following considerations. According to (9), the transformed spectrum consists of a series of peaks which decay exponentially. The position of these peaks is given by  $d = \pm mL/\pi$ . For  $m = 1$ , we get first-order peaks which correspond to the full cavity length, and for  $m > 1$ , higher order harmonics are obtained. We will use units of  $\mu\text{m}$  for the optical path length  $d$ . If there is an intracavity reflection which divides the main cavity into two subcavities,  $L = L_1 + L_2$ , then the Fourier transformed emission spectrum will reveal peaks at positions  $d_1$  and  $d_2$ , which add up to the position of the full cavity length peak at  $d = d_1 + d_2$ . As already outlined in the paragraph about the physical model, this allows the identification of cracks or other types of defects in the laser cavity.

Since, in (10), the facet reflectance and the cavity length are usually known, the only free parameter is the absorption coefficient  $k$ , which is related to the cavity propagation loss/gain. One can, therefore, determine a wavelength-averaged cavity propagation loss/gain value when performing a Fourier transform on a subthreshold emission spectrum.

For a semiconductor laser, it is further desirable to extract information about the wavelength dependence of gain from the emission spectrum. For the more complicated case in which the refractive index is still dispersion-free, but the absorption index is no longer a constant  $k = k(\beta)$ , we have to start from (7) again and do some modifications. We convinced ourselves that (7) describes the Airy function as well as (3). Furthermore, we notice that the former constant parameter  $a$  in (7) is now also a function of wavenumber  $a = a(\beta)$ . Except for this,  $a(\beta)$  is defined in exactly the same way as before via  $a = (2\pi)^{-1} \cdot (2k(\beta)L\beta_0 - \ln(R))$ . Obviously,  $a(\beta)$  occurs both inside the infinite sum, namely as a width parameter of the individual Lorentz peaks, and in front of it, as an envelope or weighting function for the series of Lorentzian peaks. If we assume that a subthreshold laser spectrum can be approximated by a series of equal-width Lorentz peaks multiplied by a wavenumber-dependent weighting function  $w(\beta')$ , then (7) becomes

$$\begin{aligned} J(\beta') &\approx \frac{C_1}{a(\beta')\pi \cdot \tanh(2a(\beta')\pi)} \cdot \sum_{m=-\infty}^{\infty} \frac{1}{1 + \left(\frac{\beta' - m}{a}\right)^2} \\ &= w(\beta') \cdot \sum_{m=-\infty}^{\infty} \frac{1}{1 + \left(\frac{\beta' - m}{a}\right)^2} \end{aligned} \quad (11)$$

where the weighting function  $w(\beta')$  is defined via

$$\begin{aligned} w(\beta') &= \frac{C_1}{a(\beta')\pi \cdot \tanh(2a(\beta')\pi)} \\ &= \left(\frac{1-R}{\sqrt{2R}}\right)^2 \cdot \frac{1}{a(\beta')\pi \cdot \sinh(2a(\beta')\pi)}. \end{aligned} \quad (12)$$

Because of the approximation introduced in (11), we can now proceed with the Fourier transform, which yields

$$\overline{I(d')} = \left[ 2\pi a \cdot e^{-2\pi a|d'|} \cdot \sum_{m=-\infty}^{\infty} \delta(d' - m) \right] \cdot W(d') \quad (13)$$

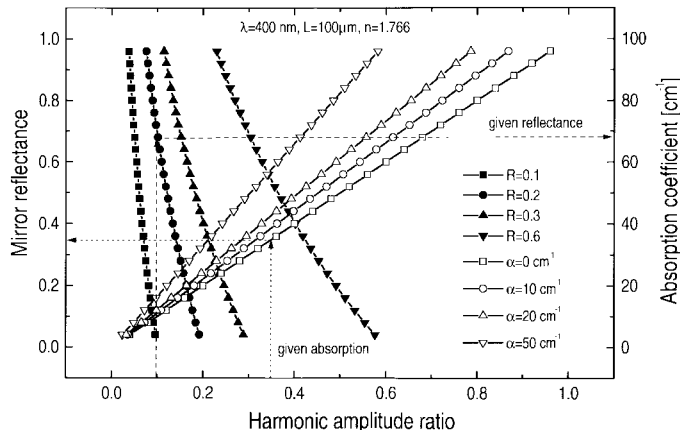


Fig. 3. Absorption loss in an active resonator for  $R = 0\%$ ,  $10\%$ ,  $20\%$ ,  $30\%$ , and  $60\%$  mirror reflectance (solid dots), and mirror reflectance of HAR. The arrows show how to figure the mirror reflectance given the absorption coefficient and vice versa.

where  $W(d')$  is the Fourier-transformed weighting function. From (13), we are able to obtain the wavelength-averaged propagation loss/gain, which is related to the exponential decay rate of the higher order harmonics. In addition, we can extract the shape of the gain curve by inverse-transforming the transformed weighting function  $W(d')$  and then solving (12) numerically for  $a(\beta')$  and  $k(\beta')$ , respectively. Usually, the measured laser spectrum is not normalized, meaning that the weighting function  $w(\beta')$  is multiplied by a constant prefactor. This ambiguity can be removed by measuring the peak gain value and adjusting the prefactor until the gain curve maximum meets this value. The peak gain value itself is being determined by Fourier-transforming a narrow spectral window in which the gain can be assumed constant.

The steps to produce such a gain spectrum using the Fourier transform technique are thus as follows. First, the emission spectrum is measured in the desired wavelength range. Then two Fourier transforms are done; one of the full spectral width and one of a narrow window (1 nm) in the central part of the spectrum which contains the gain maximum. From the full range transform, we take the (complex) data around and including the first harmonic peak. These data undergo an inverse Fourier transform in order to yield the weighting function  $w(\beta)$ . Starting from the weighting function, one solves (12) numerically and calculates  $k(\beta)$ . The boundary condition to meet the maximum gain value, as determined by the narrow window transform, can always be fulfilled by choosing an arbitrary prefactor in front of the weighting function.

According to what we derived in (1), we present in Fig. 3 a nomogram which reveals the relationship between mirror loss, absorption loss, and the harmonic amplitude ratio (HAR). The nomogram in Fig. 3 can thus be used, with measured HAR, to deduce the absorption coefficient  $\alpha$ , given the mirror power reflectance  $R$  or *vice versa*. The advantage of this method is that it can be used for both low and high finesse resonators. This is mainly because of the Fourier transform process containing information on the overall shape of the FP fringe pattern instead of only considering their contrast (low  $Q$  limit)

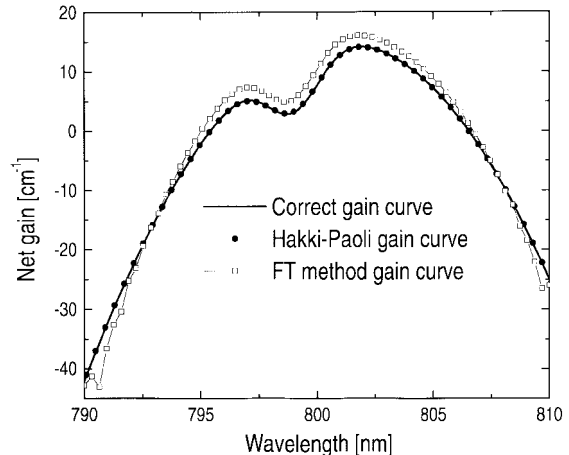


Fig. 4. Gain curves obtained from a simulated laser emission spectrum using the Hakki–Paoli method and the Fourier transform method. The initial gain curve which was used to calculate the emission spectrum is also shown (labeled “correct gain curve”).

or their peak width/separation ratio (high  $Q$  limit). Assuming an experimental spectral resolution of  $\Delta\lambda_{\text{res}} = 0.45 \text{ \AA}$ , and the mode separation of a typical blue light emitter ( $\Delta\lambda = 4.5 \text{ \AA}$ ), we are able to determine classically a resonator finesse of  $F = \Delta\lambda/\Delta\lambda_{\text{res}} = 10$ . Since the relevant information of the spectrum is in fact the shape of the transmission peaks rather than their width and separation, it is likely that using the same experimental setup as described in the next section and the Fourier transform-based measurement technique should enable us to evaluate even higher finesse FP resonators very accurately.

In Fig. 4, we show the results of using a simulated gain curve to generate a simulated emission spectrum using (3), and from this simulated emission spectrum extracting the inferred gain spectrum using both the Hakki–Paoli technique and the Fourier transform technique of this work. This provides a means to the results given by the two techniques. It is evident from this figure that the Hakki–Paoli method determines the gain very accurately if the constant offset of the spectrum is exactly known. Using the FT method gives a slight overestimation of the gain in the central part of the spectrum and an underestimation at the edge of the wavenumber range. These errors are mainly due to the assumption of having only one full-width at half-maximum (FWHM) for all cavity resonances. However, the features in the overall shape of the gain curve are well represented.

Concerning experimental limitations on both the Hakki–Paoli and Fourier transform methods, we would like to point out that Hakki–Paoli works very nicely as long as the spectrometer resolves the modes sufficiently well. However, there are principal limitations if the fringe visibility becomes close to one. Even small baseline shifts can introduce large errors in the calculation of the gain curve once this point is reached. In addition, as soon as the fringe visibility is essentially one, Hakki–Paoli does not work any more, even if a better spectrometer is used. For the Fourier transform method, since it measures the width and the shape of the fringes rather than their visibility, a better spectrometer

always helps to make the determination of the gain curve more accurate. Also, a baseline shift does not hurt at all because the dc component of the spectrum collapses into the zeroth-order harmonic peak.

#### IV. EXPERIMENTAL SETUP

We have collected experimental data with this technique using both electrically injected and optically pumped devices. The electrically injected devices were probe-tested at room temperature. Broad-area devices were tested in bar form and under pulsed conditions (800-ns pulse length, 0.08% duty cycle), whereas the infrared single-mode lasers were bonded as individual devices on copper heatsinks and operated under CW conditions. In both cases, the emitted light was collected with a microscope objective (magnification 50 $\times$ , numerical aperture 0.95) and focused onto a quartz fiber which fed onto the 50- $\mu\text{m}$ -wide slit of a high-resolution grating spectrometer (SPEX, 1.26 m focal length, 0.25  $\text{\AA}$  spectral resolution,  $\lambda = 1800$  lines/mm). Light detection was accomplished by a 1024-element array photodetector. Using this configuration, spectral measurements of a 10-nm wavelength range with a theoretical resolution of 0.1  $\text{\AA}$  could be performed. Due to the pulsed operation of the red laser diodes and the blue lasers and LED's, it was necessary to collect the light of these devices for up to 30 s. Although this collection technique is very convenient and sufficiently accurate for most applications, the noise level of this system is higher than what is in principle achievable.

The experimental setup for the optically pumped GaN-based devices was very similar to our earlier experiments [12]. It relied on the pulsed emission of a 337-nm  $\text{N}_2$  laser, which was focused to a 100- $\mu\text{m}$ -wide and 4-mm-long stripe. In order to measure output intensity versus pump intensity curves, we attenuated the pump beam with an appropriate number of 1-mm-thick glass slides which acted as neutral density filters for the  $\text{N}_2$  laser emission wavelength. The emission of the blue laser was then collected by a microscope objective, in the same manner as described above.

#### V. MEASUREMENT RESULTS

##### A. Red Broad-Area Lasers

In order to show how well this simple analysis applies to experimental data, we present here spectral measurements of GaInP–AlGaInP-based red broad-area diode lasers [21], [22] which will be compared with calculations. The laser material was a conventional red laser structure with 500-nm-thick  $\text{Al}_{0.5}\text{In}_{0.5}\text{P}$  cladding layers, a 240-nm-thick  $(\text{Al}_{0.6}\text{Ga}_{0.4})_{0.5}\text{In}_{0.5}\text{P}$  waveguide core with an 8-nm-thick GaInP quantum well in the center. It was grown on a 10 $^\circ$  misoriented GaAs substrate by metalorganic chemical vapor deposition (MOCVD). The emission wavelength of these devices was 670 nm, corresponding to a Ga mole fraction of 0.4 in the alloy composition  $\text{Ga}_x\text{In}_{1-x}\text{P}$  of the quantum well. After deposition of 50- $\mu\text{m}$ -wide Ti–Au stripes to form broad-area p-contacts, and Au–Ge n-contact metallurgy, 450- $\mu\text{m}$ -long laser bars were cleaved from the material.

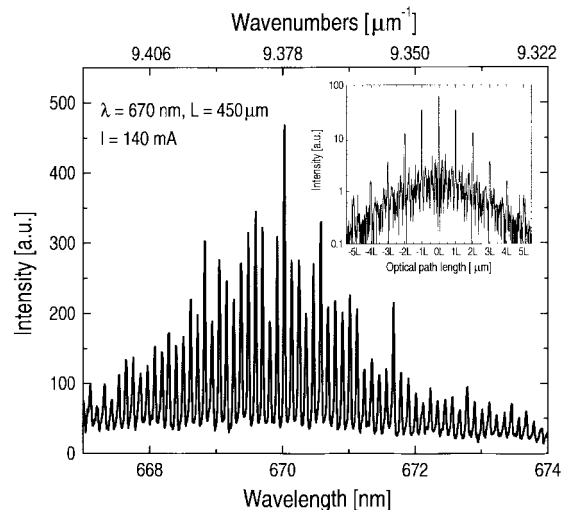


Fig. 5. High-resolution laser spectrum of a red laser at  $0.933 \cdot I_{\text{th}}$ . The inset shows Fourier transform of this spectrum.

In this paper, we measured spectra of a red broad-area laser at four different injection currents (120, 130, 140, and 150 mA) corresponding to 0.8, 0.867, 0.933, and  $1 \times I_{\text{th}}$ . A typical emission spectrum is shown in Fig. 5; it shows an FP mode spacing of 1.1  $\text{\AA}$ , corresponding to 450- $\mu\text{m}$  cavity length. This spectrum was obtained at an injection current of 140 mA ( $0.933 \times I_{\text{th}}$ ). The numerical Fourier transform of this spectrum is shown as an inset of Fig. 5. There is a main peak at  $d_0 = 450 \mu\text{m}$ , corresponding to the cavity length, and several smaller peaks at integer multiples of  $d_0$ . The presence and the slow decay rate of these peaks indicate that the  $Q$ -factor of the cavity is already high, and the shape of the individual FP modes is closer to a series of Dirac-delta functions than to a sine-function. Moreover, when choosing a logarithmic scale for the  $y$  axis, there appears to be a unique ratio between the height of adjacent peaks in the transform, i.e., the peaks of the harmonics lie on a straight line. In order to extract the peak gain value of the device, we chose a small wavelength window of only 0.5-nm width for the actual transform; this narrow spectral range transforms into a substantial broadening of the harmonic peaks in the transform domain. In Fig. 6, we compare the gain curve for 140 mA obtained by a Hakki–Paoli analysis with the gain spectrum as determined with our method. The two methods agree very well on the long-wavelength shoulder of the spectrum. Some deviations are visible on the short-wavelength side, probably because of the neglected dispersion effects in the FT method.

In order to extract the peak gain values at different injection currents, we measured the HAR  $r$  for each current level and in a narrow wavenumber window and determined the cavity propagation loss/gain by using the formula  $r = R \cdot \exp(-(\alpha - g)L)$ . The facet reflectivity  $R$  is known from the literature [23]. For this particular device, the threshold current was roughly at 150 mA. As mentioned in the theory section, the analysis does not allow the extraction of the propagation loss at threshold. For the investigated injection currents (120, 130, 140, and 150 mA), we determined loss/gain values of  $-4.05$ ,  $1.43$ ,  $7.48$ , and  $11.79 \text{ cm}^{-1}$ , respectively. These values are

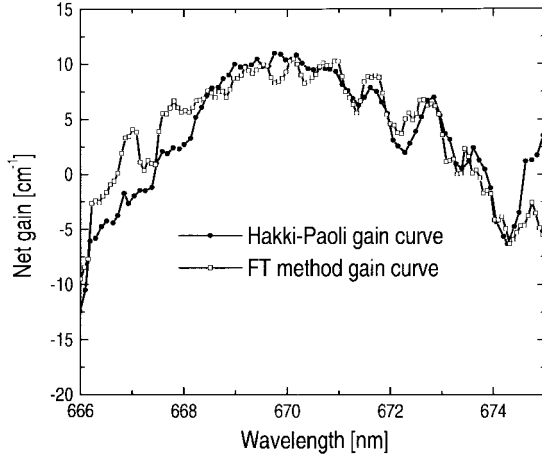


Fig. 6. Comparison between gain curves obtained with the Hakki-Paoli and the Fourier transform methods for a 450- $\mu\text{m}$ -long red broad-area laser.

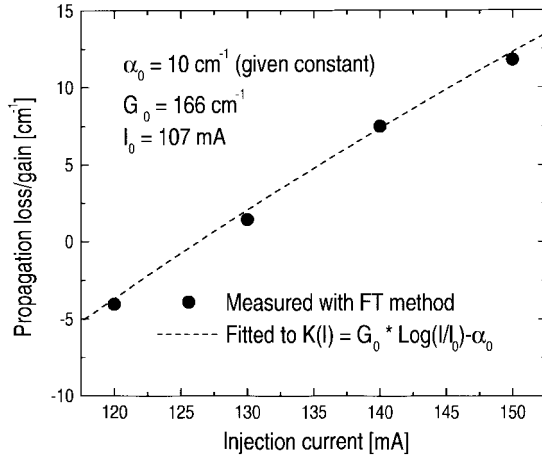


Fig. 7. Cavity propagation loss/gain versus injection current for a 450- $\mu\text{m}$ -long red broad-area laser. The fitted line assumes a logarithmic gain/current behavior.

represented by dots in Fig. 7. The dashed line is a fit of the curve  $K(I) = G_0 \cdot \log(I/I_0) - \alpha_0$  through these points, where  $\alpha_0 = 10 \text{ cm}^{-1}$  is known from an independent cavity length study [24]. The values we obtain when performing this fit are  $I_0 = 107 \text{ mA}$  and  $G_0 = 166 \text{ cm}^{-1}$ . The injection current  $I_0$  is called the transparency current level. At this current, which was determined to be at 107 mA, there is no gain in the laser cavity; it is thus characterized by  $g = 0$ .

### B. IR Laser Devices

The IR lasers tested with our technique were buried heterostructure lasers with a single-mode waveguide defined by impurity-induced layer disordering [25]. The lasers have a cavity length of 260  $\mu\text{m}$  and typical threshold currents of around 12 mA; the emission wavelength is 840 nm. These devices show, at least at certain pump levels below threshold, TE/TM- polarized longitudinal mode families of comparable intensity. Although we were able to distinguish between their slightly different refractive indices, it was not possible to resolve the resulting twin peaks in the transform unambiguously. Since the refractive index difference is only on the order of

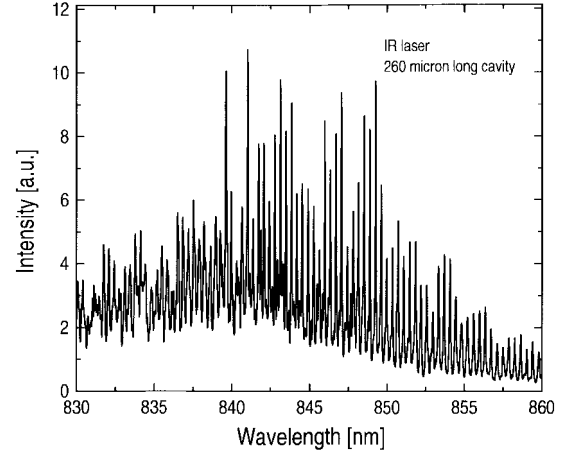


Fig. 8. Emission spectrum of an IR laser operated at 9 mA injection current. The TE/TM mode families are distinguishable.

2.5%, a resolution of at least  $0.1 \text{ \AA}$  is required in order to see clearly the twin peaks in the transform. For the first-order twin peak, this is, because of the width of the individual peaks, almost impossible. At higher pump levels, where higher order harmonics become stronger, the TM peaks are suppressed by almost an order of magnitude, which makes it again very difficult to resolve TE versus TM structure. At lower pump levels, however, the higher order harmonics decay too fast and therefore disappear in the noisy background. Given both the narrow wavelength window and the small difference in mode spacing, we were not able to distinguish the two peak families in the Fourier transform. However, we could measure the peak gain value with the Fourier transform method, although the two mode families being present at the same time prevented us from correctly determining the fringe visibility required for the Hakki-Paoli method.

We show in Fig. 8 the spectrum and in Fig. 9 three gain spectra for representative current levels of such a device. The blue shift of the gain peak at increasing injection current levels in Fig. 9 is characteristic for band-filling effects. In Fig. 10, we present the propagation loss/gain values obtained from HAR measurements on transformed emission spectra. We measured the propagation loss/gain in current steps of 0.5 mA from 8 up to 11.5 mA. Again, from an independent measurement of the absorption loss, we set  $\alpha_0 = 5 \text{ cm}^{-1}$  [26]. The fit through these points, similar to Fig. 7, results in  $I_0 = 7.6 \text{ mA}$ , and  $G_0 = 226 \text{ cm}^{-1}$ .

### C. Blue LED's

In this class of devices, we analyzed the emission spectrum of an AlGaInN double-heterostructure which is grown on a 100- $\mu\text{m}$ -thick sapphire substrate. The 5- $\mu\text{m}$ -thick epitaxial layers have an average refractive index of 2.51; the refractive index of sapphire is 1.77. Due to the reflections at the GaN surface, the GaN-sapphire interface, and the sapphire surface, three different FP cavities were formed. However, only two of them show up as closely spaced peaks in the Fourier-transformed emission spectrum of this device. The third peak is too close to the origin to be resolved, mainly because of the large mode spacing ( $\Delta\lambda = 5.3 \text{ nm}$ ) of the AlGaInN cavity.

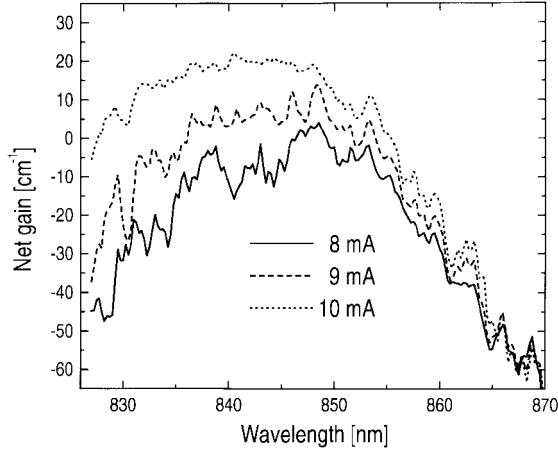


Fig. 9. Gain curves for three different current levels of a 260- $\mu\text{m}$ -long IR laser. The curves are measured using the Fourier transform technique.

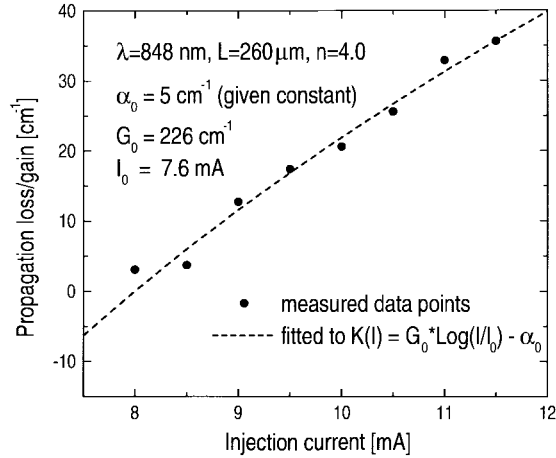


Fig. 10. Cavity propagation loss/gain versus injection current for a 260- $\mu\text{m}$ -long IR single-mode buried heterostructure laser. The fitted line assumes a logarithmic gain/current behavior.

A typical emission spectrum and its Fourier transform are shown in Fig. 11. By extracting a HAR of 0.1, and assuming an average mirror reflectance of 10%, an averaged cavity propagation loss of approximately  $1 \text{ cm}^{-1}$  can be found. This assumes that the cavity loss in this case is entirely due to distributed cavity loss. It is also possible, however, that in this case, scattering losses at the surfaces are also high, resulting in discrete lossy planes at, for example, the GaN-sapphire interface. This example shows the danger of assuming that the presence of pronounced FP modes indicates that a device is close to threshold. In the example, the device has just reached the transparency condition ( $g = 0$ ) and might still be far from threshold.

#### D. Pits and Cracks in Blue Optically Pumped Lasers

For these experiments, we used undoped MOCVD-grown samples with a 4- $\mu\text{m}$ -thick GaN buffer, a 500-nm AlGaIn lower clad, a 240-nm GaN waveguide with five InGaIn QW's, and a 50-nm-thick upper clad on top. We investigated both samples where cracks were visible and samples in which we did not expect cracks. The 510- $\mu\text{m}$ -long laser cavities were

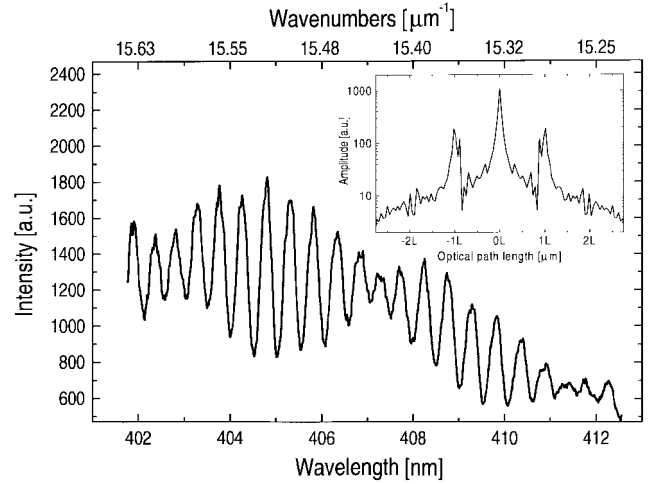


Fig. 11. Emission spectrum of a blue GaN LED. The inset shows the Fourier transform of the spectrum. The twin peaks are due to multiple reflections at the GaN-sapphire interface.

formed by two polished facets and a high reflectivity (HR) Al-mirror on one side ( $R = 93\%$ ). A 5- $\mu\text{m}$ -wide and 300-nm-deep groove was dry etched into a sample that we did not expect to be cracked. The etched groove was oriented at a shallow angle to the emitting facets and divided the main cavity into two shorter subcavities of variable length. At position A, there was no etched groove. At a different position B, the two subcavities were 200 and 310  $\mu\text{m}$  long, respectively. At a position C, they finally measured 240 and 270  $\mu\text{m}$ .

Fourier transforms of the laser spectra of the devices at positions A, B, and C allowed us to compare the effect of the etched groove and the crystal imperfections on the laser spectrum [27]. Obviously, the etched groove and those reflecting features which give sufficient backscattering into the waveguide mode serve as additional parasitic mirrors within the laser cavity. Each additional reflection forms its own two FP subcavities; one with the back and one with the front facet. If there is more than one intra-cavity reflection, then there are even more possibilities for the formation of subcavities. Let us assume here for simplicity that each feature produces only one pair of subcavities. We therefore expect for each of these subcavities its own FP mode spacing, corresponding to one peak pair in the Fourier transform of the emission spectrum.

We measured the emission spectra of the above sample at a position beyond the etched groove (position A), and at two further positions within the grooved region (positions B and C). Fig. 12 shows the Fourier transformed emission spectrum of the unperturbed laser cavity at position A and, as an inset, the emission spectrum itself. There are clearly visible FP oscillations in the spectrum which give rise to very pronounced cavity length peaks at around 510  $\mu\text{m}$  in the transform. The origin of this peak family instead of a single peak is a result of filamenting in the laser cavity. Since the films were grown without rotation of the sapphire substrate, there is a substantial thickness gradient across the wafer leading to different emission wavelengths for the various lasing filaments.

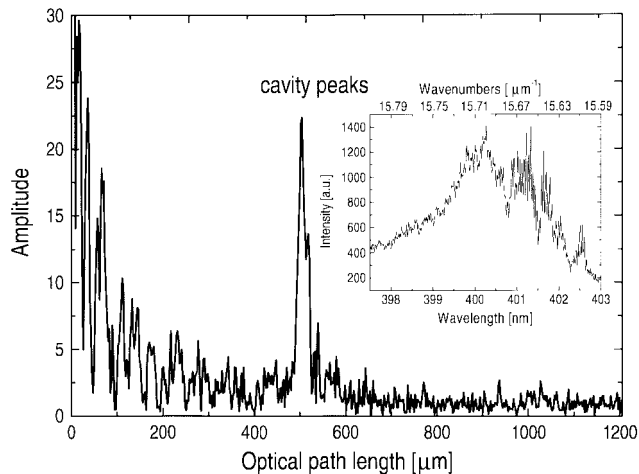


Fig. 12. Fourier-transformed emission spectrum of an optically pumped blue laser measured beyond the grooved region. The spectrum, which is shown as an inset, was measured with a high-resolution spectrometer.

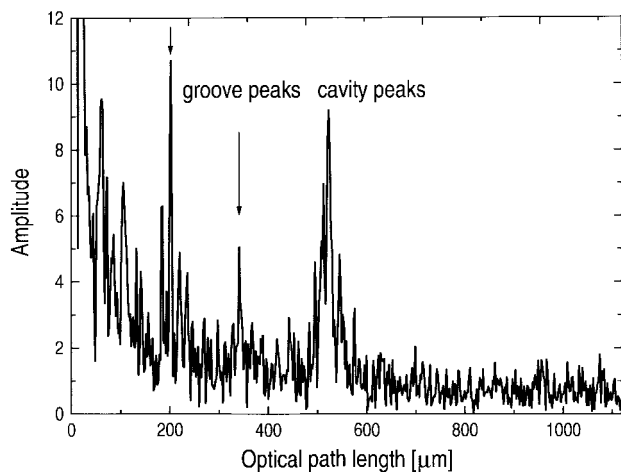


Fig. 13. Fourier-transformed spectrum from the grooved area. The peak pair corresponding to the etched groove is marked by arrows.

A measurement of the emission spectra at positions B and C resulted typically in Fourier transforms as shown in Fig. 13. Both of them revealed peak pairs whose inverse spacings were clearly related to the distance to the grooved facet for each particular position. This establishes that the etched groove adds additional peaks to the transform of the existing laser spectrum, at positions determined by the position of the etched groove within the cavity.

There are many other features in the transform spectrum with optical path lengths below  $510 \mu\text{m}$ . This structure must be due to additional perturbations within the laser cavity. We have seen data for which the inverse mode separations of pairs of these additional peaks add up to the mode spacing of the full cavity length peak, as described above. This implies the presence of discrete scattering centers at specific locations within the cavity. The TEM investigation of this sample revealed hexagonally shaped 300-nm-deep and 250-nm-wide pits that extended from the surface into the active layer. By doing an AFM surface scan, we found an average pit-to-pit distance of  $2 \mu\text{m}$ . This figure, taken by itself, is

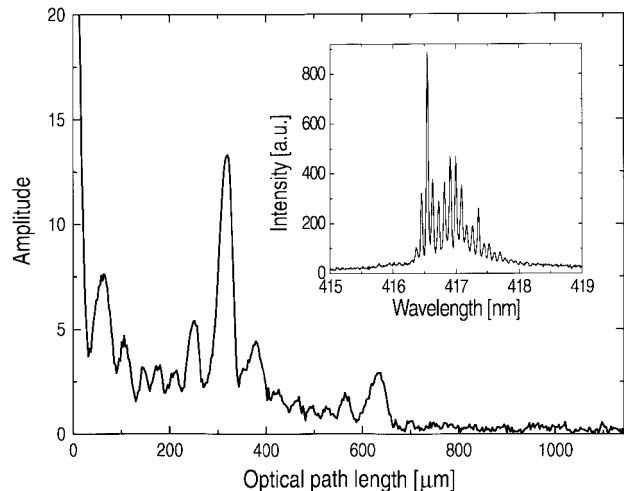


Fig. 14. Fourier-transformed emission spectrum of a 300- $\mu\text{m}$ -long electrically pumped blue laser diode. The regular structures occurring at optical path lengths below the cavity length are due to the optical coupling between laser waveguide and substrate waveguide. The inset shows the spectrum with the gain modulations which are responsible for the intracavity peaks.

higher than the density of scatterers given by the number of reflection peaks. However, it is likely that the laser filaments are established along lines which minimize scattering loss and therefore minimize the number of pit intersections. In addition, it is possible that some number of pits do not backscatter into the waveguide mode.

As a comparison, we show in Fig. 14 the Fourier-transformed emission spectrum of an electrically pumped blue laser device below threshold. The regularly spaced peaks occurring between the harmonic peaks are due to the coupling between laser waveguide and substrate waveguide. This effect causes a gain variation, which modulates the emission spectrum with a period of five to six FP mode spacings [28]. Taking into account the greatly improved material quality and the fact that only very little noise is visible between the harmonic peaks, it becomes obvious that the fine structure in Figs. 12 and 13 is not due to noise but rather due to scattering centers within the laser cavity.

## VI. CONCLUSIONS

We have shown a new powerful method for the quantitative and qualitative analysis of laser resonators in terms of propagation loss/gain. The method is based on Fourier analysis of subthreshold laser spectra and measurement of the relative amplitude of adjacent higher order harmonics in these Fourier transforms. As a result of this, we have measured gain spectra of red/infrared semiconductor lasers using the Fourier transform method and compared them with Hakki-Paoli gain spectra. We also obtained information about the origin of scattering loss, especially with respect to devices in the gallium nitride material system. The main loss mechanism in the laser cavity of our AlGaInN-based laser material appeared to be pits in the surface which penetrate to the active region. Since the laser oscillates in narrow filaments, even relatively small pits can cause a strong backreflection resulting in the insertion of fine structure into the Fourier transformed spectrum. Since

our method requires only simple processing, it offers an important diagnostic technique for the evaluation of the structural integrity of the optical waveguide.

#### ACKNOWLEDGMENT

The authors are grateful to D. P. Bour, D. W. Treat, and H. F. Chung for crystal growth, D. Sun, and R. Donaldson for device fabrication, F. Endicott, D. F. Fork, and G. Anderson for setting up the experiment, M. K. W. Seifert from the Mathematics Department of the University of California at Irvine for his help in some of the calculations, and R. D. Bringans and T. L. Paoli for helpful discussions and support.

#### REFERENCES

- [1] B. W. Hakki and T. L. Paoli, "CW degradation at 300 K of GaAs double-heterostructure junction lasers. II. Electronic gain," *J. Appl. Phys.*, vol. 44, no. 9, pp. 4113–4119, 1973.
- [2] ———, "Gain spectra in GaAs double-heterostructure injection lasers," *J. Appl. Phys.*, vol. 46, no. 3, pp. 1299–1306, 1975.
- [3] M. Born and E. Wolf, *Interference and Interferometers, Principles of Optics*, 6th ed. New York: Pergamon, 1984, vol. 256.
- [4] B. D. Patterson, C. Musil, H. Siegwart, and A. Vonlanthen, "Focused-ion beam modification of waveguide photonic devices," *Microelect. Eng.*, vol. 27, pp. 347–350, 1995.
- [5] B. D. Patterson, "Characterization of active waveguide photonic devices using optical coherence domain reflectometry," *Opt. Eng.*, vol. 34, no. 8, pp. 2289–2298, 1995.
- [6] V. G. Cooper, "Analysis of Fabry–Perot in erferograms by means of their Fourier transforms," *Appl. Opt.*, vol. 10, no. 3, pp. 525–530, 1971.
- [7] D. M. Rust, "Etalon filters," *Opt. Eng.*, vol. 33, no. 10, pp. 3342–3348, 1994.
- [8] W. B. Cook, H. E. Snell, and P. B. Hays, "Multiplex-Fabry–Perot interferometers: I. Theory," *Appl. Opt.*, vol. 34, no. 24, pp. 5263–5267, 1995.
- [9] Z. L. Liao, R. L. Aggarwal, P. A. Maki, R. J. Molnar, J. N. Walpole, R. C. Williamson, and I. Melngailis, "Light scattering in high-dislocation density GaN," *Appl. Phys. Lett.*, vol. 69, no. 12, pp. 1665–1667, 1996.
- [10] L. T. Romano, B. S. Krusor, W. Götz, N. M. Johnson, R. J. Molnar, and E. Brown, "Structural characterization of thick GaN films grown by hydride vapor phase epitaxy," in *Proc. Materials Research Society*, 1996, vol. 423, pp. 500–505.
- [11] F. A. Ponce, B. S. Krusor, J. S. Major, Jr., W. E. Plano, and D. F. Welch, "Microstructure of GaN epitaxy on SiC using AlN buffer layers," *Appl. Phys. Lett.*, vol. 67, no. 3, pp. 410–412, 1995.
- [12] D. Hofstetter, D. P. Bour, R. L. Thornton, and N. M. Johnson, "Excitation of a higher order transverse mode in an optically pumped  $\text{In}_{0.15}\text{Ga}_{0.85}\text{N}/\text{In}_{0.05}\text{Ga}_{0.95}\text{N}$  multiquantum well laser structure," *Appl. Phys. Lett.*, vol. 70, no. 13, pp. 1650–1652, 1997.
- [13] S. T. Kim, H. Amano, and I. Akasaki, "Surface-mode stimulated emission from optically pumped GaInN at room temperature," *Appl. Phys. Lett.*, vol. 67, no. 2, pp. 267–269, 1995.
- [14] T. J. Schmidt, X. H. Yang, W. Shan, J. J. Song, A. Salvador, W. Kim, Ö. Aktas, A. Botchkarev, and H. Morkoç, "Room-temperature stimulated emission in GaN/AlGaIn separate confinement heterostructures grown by molecular beam epitaxy," *Appl. Phys. Lett.*, vol. 68, no. 7, pp. 1820–1822, 1996.
- [15] A. S. Zubrilov, V. I. Nikolaev, V. A. Dmitriev, K. G. Irvine, J. A. Edmond, and C. H. Carter, Jr., "Stimulated emission from GaN grown on SiC," in *Inst. Phys. Conf. Ser.*, 1994, vol. 141, pp. 525–530.
- [16] D. Hofstetter and R. L. Thornton, "Theory of loss measurements on Fabry–Perot resonators by Fourier analysis of the transmission spectra," *Opt. Lett.*, vol. 12, no. 24, pp. 1831–1833, 1997.
- [17] D. Hofstetter and R. L. Thornton, "Loss measurements on semiconductor lasers by Fourier analysis of the emission spectra," *Appl. Phys. Lett.*, vol. 72, no. 4, pp. 404–406, 1998.
- [18] R. N. Bracewell, *The Fourier Transform and its Applications*, 2nd ed. New York: McGraw-Hill, 1986, pp. 267–272.
- [19] E. Hecht and A. Zajac, *Optics*, 3rd ed. Reading, MA: Addison Wesley, 1976, vol. 307.
- [20] W. H. Steel, *Interferometry*, 2nd ed. Cambridge, U.K.: Cambridge Univ., 1983, ch. 9, pp. 141–149.
- [21] D. P. Bour, R. S. Geels, D. W. Treat, T. L. Paoli, F. A. Ponce, R. L. Thornton, B. S. Krusor, R. D. Bringans, and D. F. Welch, "Strained  $\text{Ga}_x\text{In}_{1-x}\text{P}/(\text{AlGa})_{0.5}\text{In}_{0.5}$  heterostructures and quantum well laser diodes," *IEEE J. Quantum Electron.*, vol. 30, pp. 593–607, 1994.
- [22] D. P. Bour, D. W. Treat, R. L. Thornton, T. L. Paoli, R. D. Bringans, B. S. Krusor, R. S. Geels, D. F. Welch, and T. Y. Wang, "Low threshold  $\text{Ga}_x\text{In}_{1-x}\text{P}/(\text{Al}_y\text{Ga}_{1-y})_{0.5}\text{In}_{0.5}\text{P}$  strained quantum well lasers," *J. Cryst. Growth*, vol. 124, no. 3, pp. 751–756, 1992.
- [23] I. P. Kaminow, G. Eisenstein, and L. W. Stulz, "Measurement of the modal reflectivity of an antireflection coating on a superluminescent diode," *IEEE J. Quantum Electron.*, vol. QE-19, pp. 493–495, Apr. 1983.
- [24] D. P. Bour and G. A. Evans, "Lateral mode discrimination in AlGaInP selectively buried ridge waveguide lasers," *Proc. Inst. Elect. Eng.*, vol. 139, no. 1, pp. 71–74, 1992.
- [25] R. L. Thornton, R. D. Burnham, T. L. Paoli, N. Holonyak, Jr., and D. G. Deppe, "Low threshold planar buried heterostructure lasers fabricated by impurity-induced disordering," *Appl. Phys., Lett.*, vol. 47, no. 12, pp. 1239–1241, 1985.
- [26] R. L. Thornton, T. L. Paoli, and F. Endicott, private communication.
- [27] B. D. Patterson, J. E. Epler, B. Graf, H. W. Lehmann, and H. C. Sigg, "A superluminescent diode at 1.3  $\mu\text{m}$  with very low spectral modulation," *IEEE J. Quantum Electron.*, vol. 30, pp. 703–712, Mar. 1994.
- [28] I. A. Arvutsky, R. Gordon, R. Clayton, and J. M. Xu, "Investigations of the spectral characteristics of 980 nm InGaAs-GaAs-AlGaAs lasers," *IEEE J. Quantum Electron.*, vol. 33, pp. 1801–1809, Oct. 1997.

**Daniel Hofstetter** was born in Zug, Switzerland, in 1966. He received the Dipl. Phys. ETH degree in physics from the Swiss National Institute of Technology (ETH) in 1993. His diploma thesis, entitled "CO-laser photo-acoustic spectroscopy of fatty acid vapors," was directed by Prof. F. K. Kneubühl and Prof. M. W. Sigrist from the Infrared Laboratory of the ETH in Zurich. He received the Ph.D. degree in physics from the University of Neuchâtel in 1996. His dissertation about monolithically integrated displacement sensors for optical displacement measurement, which was carried out und the supervision of Prof. R. Dänkliker and Dr. H. P. Zappe, was awarded the prize of the Swiss Physical Society in 1997.

After an apprenticeship at Landis & Gyr, Zug, Switzerland, as an Electrical Mechanic from 1982 to 1986, he was employed at the same company as a Physics Technician. From 1996 to 1998, he worked at the Xerox Palo Alto Research Center, Palo Alto, CA, where he was involved with the fabrication and testing of AlGaInN DFB lasers and the integration of multicolor lasers for scanning applications. He is currently with the Physics Department, Neuchâtel University, Neuchâtel, Switzerland, developing long-wavelength quantum cascade DFB lasers.

**Robert L. Thornton** (M'85) was born in Washington, DC, in 1955. He received the B.S. degree from the California Institute of Technology, Pasadena, in 1978, and the Ph.D. degree from Stanford University, Stanford, CA, in 1983, where he performed research on nonlinear signal processing devices using surface acoustic waves.

In 1983, he became a Member of the Research Staff at Xerox Palo Alto Research Center, Palo Alto, CA. He was promoted to Principal Scientist in 1991. His work at Xerox, conducting research on semiconductor laser device technology, has resulted in more than 30 patents and over 100 technical publications. In 1998, he became the Director of Photonic Technology at Maxtek Components Corporation, Beaverton, OR, where he is responsible for guiding technology selection and development in the areas of semiconductor lasers, photodetectors, and architectures for integrated optoelectronics.

Dr. Thornton is a member of the American Physical Society.